Enhanced photocatalytic CO_2 reduction via single-atom Au anchored on $ZnIn_2S_4$ nanosheets

Zhaoyang Zhang[1], Houdong Rao[2], Dongyang Zhang[3], Ling Zhang[4], Wei Cheng[5]
Luoyang Ship Material Research Institute, Luoyang, 471023, China
[2]Corresponding author
E-mail: [1]*815987591@qq.com*, [2]*q8rao8@163.com*, [3]*zdy_dut@163.com*, [4]*zhangling918813@163.com*, [5]*chengwei@725.com.cn*

Received 22 January 2024; accepted 17 February 2024; published online 4 April 2024
DOI https://doi.org/10.21595/vp.2024.23948

68th International Conference on Vibroengineering in Almaty, Kazakhstan, April 4-6, 2024

Abstract. In this study, we systematically investigated the effect of single-atom gold (Au) loaded on $ZnIn_2S_4$ nanosheets on the photocatalytic reduction of carbon dioxide (CO_2). Utilizing a photodeposition method, we successfully dispersed single-atom Au uniformly on the surface of $ZnIn_2S_4$ nanosheets. Under simulated sunlight irradiation, the Au-loaded catalyst demonstrated a higher yield and selectivity in the CO_2 reduction reaction compared to the pure $ZnIn_2S_4$ nanosheets. Surface photovoltage testing revealed that the addition of Au significantly enhanced the separation efficiency of photo-generated charge carriers, thereby improving the photocatalytic efficiency. Density functional theory calculations indicated that the loading of single-atom Au reduced the reaction energy barrier from CO_2 to CO, enhancing the selectivity of photocatalytic CO_2 reduction. This research not only developed an efficient catalyst for CO_2 reduction but also provided deep insights into the mechanism of single-atom catalysts in the photocatalytic CO_2 reduction process through extensive experimental and theoretical analysis.

Keywords: single-atom Au, zinc indium sulfide, nanosheets, photocatalysis, CO_2 reduction.

1. Introduction

In recent years, with the increasing severity of global climate change and the energy crisis, photocatalytic carbon dioxide (CO_2) reduction technology has garnered widespread attention in the scientific community as a method to convert CO_2 into useful fuels or chemicals [1, 2]. This technology not only holds the promise of mitigating greenhouse gas emissions but also converting and storing solar energy, thereby realizing a sustainable energy cycle. Among various studies, the development of efficient, stable, and cost-effective photocatalysts represents a core challenge in advancing the practical application of photocatalytic CO_2 reduction technology [3-6]. In this context, $ZnIn_2S_4$, a widely studied photocatalytic material, is favored for its excellent light absorption properties and stable chemical characteristics. However, its photocatalytic efficiency in practical applications still requires enhancement [7-9].

Single-atom catalysts have recently gained significant attention in the field of photocatalysis due to their unique properties at the atomic scale, particularly their unique electronic structures and maximized atomic utilization efficiency [10-12]. Single-atom gold (Au), as an active co-catalyst, has demonstrated superior performance in various domains [13]. In photocatalytic CO_2 reduction and other reactions, single-atom gold significantly improves the kinetics and thermodynamics of the reaction by adjusting the electronic density of the catalyst's surface and providing unique adsorption sites. This not only enhances the catalyst's activity but also increases the selectivity of the products, crucial for efficient conversion and production of specific chemicals [14, 15].

In this research, we applied photodeposition to uniformly distribute single-atom gold (Au) on $ZnIn_2S_4$ nanosheets, creating an effective photocatalyst. We found that single-atom Au notably enhanced the rate and selectivity of CO_2 reduction compared to the pristine $ZnIn_2S_4$. Surface photovoltage tests indicated that single-atom Au significantly improves charge separation, thus

boosting catalytic efficiency. Density functional theory (DFT) calculations showed that Au loading lowers the energy barrier for converting CO_2 to CO, enhancing photocatalytic CO_2 reduction selectivity. This study advances our understanding of single-atom catalysts in photocatalysis and offers valuable insights for the development of more efficient photocatalytic systems.

2. Experiment

2.1. Synthesis of catalyst

2.1.1. Laboratory reagents

Zinc chloride (98 %), Indium chloride tetrahydrate (98 %), $HAuCl_4$ (98 %) and thioacetamide were purchased from Beijing Inokai Technology Co., LTD. All the ultrapure water used in the experiment was prepared by the ultrapure water machine Milli-Q Biocel.

2.1.2. Sample preparation

Zinc Indium Sulfide Nanosheets (ZIS): In a typical synthesis, 0.4 mmol of Zinc Chloride (ZnCl2), 0.8 mmol of Indium Chloride Tetrahydrate (InCl3·4H2O), and 3.2 mmol of Thiourea were successively dissolved in a solvent mixture containing 15 mL of deionized water and 15 mL of ethanol, under vigorous stirring for 5 minutes. Subsequently, the mixture was transferred to a 40 mL capacity Teflon-lined autoclave, sealed, and subjected to hydrothermal reaction at 180 °C for 24 hours. After completion, the system was naturally cooled to room temperature. The resultant product was centrifuged, washed thrice with deionized water and ethanol, and then dried overnight under vacuum at 60 °C. To exfoliate the product into ultrathin nanosheets, 20 mg of the product was dispersed in 30 mL of deionized water and ultrasonicated for 30 minutes using a Branson SFX250 Sonifier. The exfoliated nanosheets were then collected and dried under vacuum at 40 °C for 12 hours. Finally, the dispersion was dried under vacuum at 40 °C for 12 hours to obtain the final product.

Gold-Loaded Zinc Indium Sulfide Nanosheets (Au-ZIS): To synthesize Au-ZIS, a photochemical deposition method was adopted. In a typical process, 100 mg of ZIS and 1.2 mg of HAuCl4 were dispersed in 100 mL of ethanol. The suspension was then transferred into a sealed quartz container. Prior to illumination, the system was purged with argon gas for 30 minutes to completely displace air in the system. At 25°C, a 300-watt xenon lamp (Beijing PerfectLight MICROSOLAR 300) was used as the light source for a 30-minute photochemical deposition. The catalyst loaded with Au was collected by centrifugation and washed three times with deionized water, followed by vacuum drying at 40 °C for 12 hours.

2.2. Performance and characterization of samples

In typical activity tests, 10 mg of the photocatalyst is dispersed in deionized water and then uniformly spread over a 3 cm diameter microfiber filter paper (WHATMAN, QMA 1851-047) using a vacuum filter. The microfiber filter paper bearing the photocatalyst is placed inside a 100 mL high-pressure reactor with a quartz window on the top. Before illumination, 0.3 mL of triethanolamine and 0.3 mL of deionized water are injected into the system, followed by three vacuum cycles of the photoreactor. Subsequently, the reactor is filled with carbon dioxide gas until the pressure reaches 0.2 MPa. A 300 W xenon lamp is used as the light source. During the reaction, gas products are analyzed using a gas chromatograph (GC7920-TF2Z) equipped with a thermal conductivity detector and a flame ionization detector.

3. Results and discussion

3.1. Characterization and analysis of surface structure

Firstly, to comprehensively understand the morphology and structural characteristics of the synthesized $ZnIn_2S_4$ (ZIS) nanosheets, we employed Transmission Electron Microscopy (TEM) for preliminary analysis. The TEM images (Fig. 1(a)) depict the ZIS nanosheets as having a regular, flake-like distribution with uniform size and distinct edges. Furthermore, to delve into the lattice structure in detail, High-Resolution Transmission Electron Microscopy (HRTEM) was utilized for in-depth observation. As illustrated in Fig. 1(b), we observed that the lattice spacing of the ZIS catalyst is 0.331 nm, revealing that the nanosheets predominantly expose the (100) crystal facet, implying potential active facets and superior catalytic performance [16]. To confirm the chemical composition and uniform distribution of elements in ZIS, Energy-Dispersive X-ray Spectroscopy (EDS) was further conducted for elemental analysis. The EDS maps (Fig. 1(c-f)) clearly display the presence of indium (In), zinc (Zn), and sulfur (S) elements, uniformly distributed without any other impurity elements detected. These results confirm the successful synthesis of zinc indium sulfide.

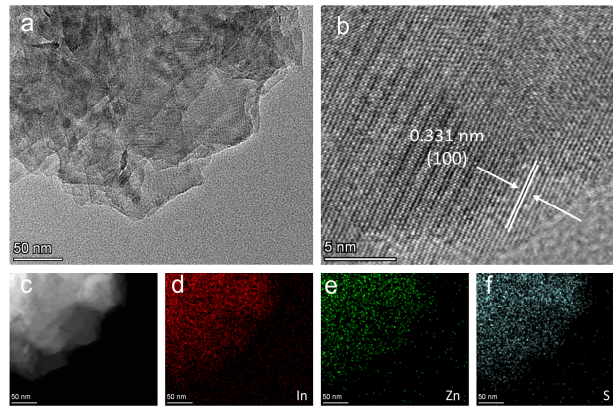

Fig. 1. a) TEM image, b) HRTEM image and c-f) EDS mapping of ZIS

Based on ZIS, we employed a photo-deposition method to load gold (Au) onto ZIS, resulting in gold-loaded ZIS nanosheets (Au-ZIS). Detailed characterizations were conducted on the Au-ZIS. Initially, Transmission Electron Microscopy (TEM) analysis (Fig. 2(a)) indicated that the Au-loaded ZIS nanosheets maintained their original flake-like structure and size uniformity, suggesting that the photo-deposition process did not significantly alter the morphology of the ZIS nanosheets. Further observation through High-Resolution Transmission Electron Microscopy (HRTEM) (Fig. 2(b)) revealed that the lattice spacing of Au-ZIS remained consistent with that of the unmodified ZIS, implying that the loading of gold did not alter the lattice structure of ZIS. Notably, no distinct gold nanoparticles or clusters were observed in the high-resolution TEM images, hinting that gold might be uniformly dispersed on the ZIS nanosheets at an atomic level [17]. To further verify the state and distribution of gold, Energy-Dispersive X-ray Spectroscopy (EDS) (Fig. 2(c-g)) was employed. The analysis distinctly demonstrated the presence of gold (Au), indium (In), zinc (Zn), and sulfur (S), all uniformly distributed, further confirming the successful loading and excellent dispersion of gold.

To delve deeper into the distribution and presence of Au on ZIS nanosheets, this study utilized High-Angle Annular Dark-Field Scanning Transmission Electron Microscopy (HAADF-STEM) for detailed catalyst characterization. The HAADF-STEM images, owing to their high sensitivity to atomic number, allow different elements to be distinguished by varying brightness, with elements of higher atomic numbers appearing brighter. As displayed in Fig. 3(a), no formation of

gold nanoparticles or clusters was observed, indicating that gold is likely dispersed on the ZIS nanosheets in a single-atom form [18]. Further, magnified view (Fig. 3(b)) distinctly shows the distribution of individual atoms. In these images, while Zn and S atoms are less conspicuous due to their relatively lower atomic numbers, the presence of In and Au atoms is clearly visible, with Au atoms appearing as the brightest spots [19]. The positions of some Au atoms are specifically indicated by red circles on the images. These observations conclusively demonstrate that Au atoms are uniformly dispersed at the atomic level on ZIS nanosheets.

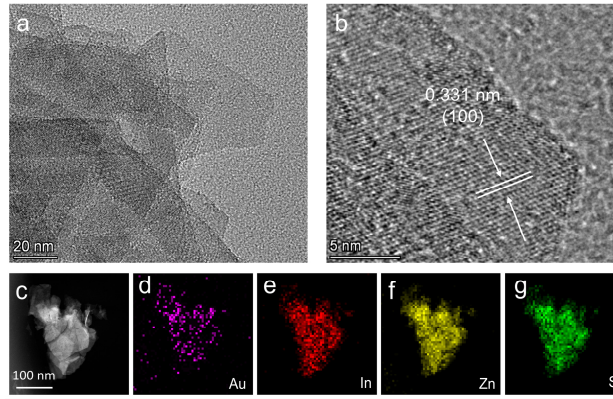

Fig. 2. a) TEM image, b) HRTEM image and c-f) EDS mapping of Au-ZIS

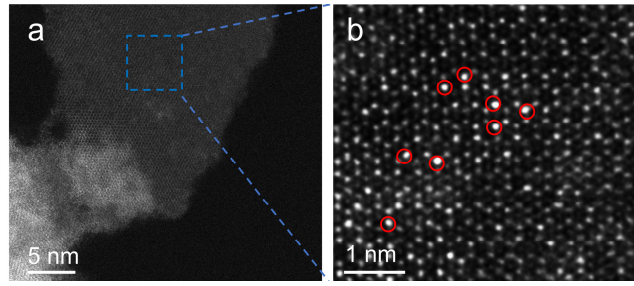

Fig. 3. HAADF-STEM for Au-ZIS

3.2. Characterization of catalytic properties of hydrogen production

We systematically characterized the photocatalytic CO_2 reduction performance of ZIS and Au-ZIS. As illustrated in Figs. 4(a) and 4(b), both Au-ZIS and ZIS primarily produced carbon monoxide (CO) and hydrogen (H_2) via photocatalytic CO_2 reduction, where CO was derived from the reduction of CO_2, and H_2 predominantly originated as a by-product from the photolysis of water. Specifically, Au-ZIS exhibited superior performance: the production rates of CO and H_2 reached 25.8 and 4.2 $\mu mol \cdot g^{-1} \cdot h^{-1}$, respectively, with CO selectivity reaching as high as 86 %. In contrast, the unmodified ZIS demonstrated relatively weaker performance with CO and H2 production rates of 12.4 and 13.6 $\mu mol \cdot g^{-1} \cdot h^{-1}$, respectively, and a CO selectivity of only 47 %. This comparison clearly indicates that depositing single-atom gold on ZIS not only significantly enhanced the overall yield of photocatalytic CO_2 reduction but, more importantly, greatly improved the selectivity towards CO.

3.3. Catalytic mechanism

It is well-recognized that the performance of photocatalysts is directly linked to the efficient separation and transfer of photogenerated electron-hole pairs [20]. Therefore, to deeply understand the reasons behind the significant enhancement of photocatalytic CO_2 reduction performance of

Au-ZIS compared to ZIS catalysts, we systematically studied the separation efficiency of photogenerated electron-hole pairs for both catalysts. Fig. 5 shows the SPV data for both Au-ZIS and ZIS catalysts. The results clearly demonstrate that the surface photovoltage of the Au-ZIS catalyst is significantly higher than that of the ZIS catalyst, indicating that the metal modification has significantly promoted the effective separation of electron-hole pairs. The enhanced separation efficiency of photogenerated electron-hole pairs means that under the same illumination conditions, the surface of the Au-ZIS catalyst can produce more free electrons to participate in the reduction of CO_2, thereby accelerating the rate of photocatalytic reaction.

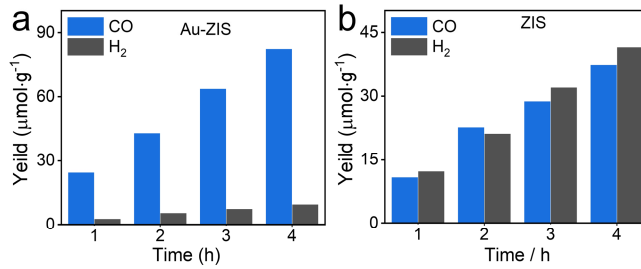

Fig. 4. Characterization of a) Au-ZIS and b) photocatalytic CO_2 reduction properties of ZIS

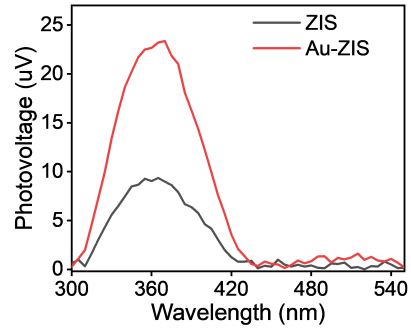

Fig. 5. Surface photovoltage test

To comprehensively understand the scientific mechanism behind the enhanced selectivity in photocatalytic carbon dioxide (CO_2) reduction of gold-doped $ZnIn_2S_4$ (referred to as Au-ZIS) compared to pure $ZnIn_2S_4$ (referred to as ZIS), this study meticulously compared the Gibbs free energy changes for the CO_2 reduction reaction from CO_2 to various potential reaction intermediates over both catalysts. As illustrated in Fig. 6, it was observed that, for Au-ZIS, the Gibbs free energy changes for all the intermediate steps were lower than those for ZIS. This indicates that the introduction of single-atom Au not only altered the electronic structure and adsorptive properties of the catalyst's surface but also reduced the reaction barriers, thereby enhancing the thermodynamic feasibility of CO_2 reduction reactions on the Au-ZIS catalyst.

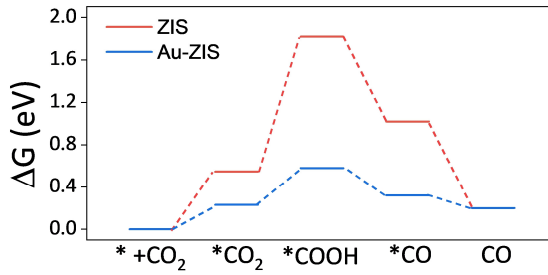

Fig. 6. Gibbs free energy change of CO_2 reduction calculated by density functional theory

ISSN PRINT 2345-0533, ISSN ONLINE 2538-8479

4. Conclusions

This study presents a thorough analysis of the superior photocatalytic CO_2 reduction performance of Au-ZIS over ZIS. It utilizes Transmission Electron Microscopy (TEM), High-Resolution TEM, Energy Dispersive X-ray Spectroscopy, and High-Angle Annular Dark-Field Scanning TEM to demonstrate that Au-ZIS maintains regular structures with well-dispersed gold atoms, without forming gold nanoparticles or clusters. Photocatalytic tests reveal that Au-ZIS achieves higher CO yield and selectivity, attributed to its enhanced charge separation efficiency confirmed by Surface Photovoltage testing. Density Functional Theory calculations indicate a more negative Gibbs free energy change for CO_2 conversion on Au-ZIS, suggesting a stronger thermodynamic driving force. This research not only synthesizes an efficient Au-ZIS photocatalyst but also elucidates its outstanding performance from structural, compositional, photoelectric, and thermodynamic perspectives, laying a foundation for designing more effective photocatalysts.

Acknowledgements

The authors have not disclosed any funding.

Data availability

The datasets generated during and/or analyzed during the current study are available from the corresponding author on reasonable request.

Conflict of interest

The authors declare that they have no conflict of interest.

References

[1] C. Hepburn et al., "The technological and economic prospects for CO2 utilization and removal," *Nature*, Vol. 575, No. 7781, pp. 87–97, Nov. 2019, https://doi.org/10.1038/s41586-019-1681-6

[2] W. Ma et al., "Promoting electrocatalytic CO2 reduction to formate via sulfur-boosting water activation on indium surfaces," *Nature Communications*, Vol. 10, No. 1, pp. 1–10, Feb. 2019, https://doi.org/10.1038/s41467-019-08805-x

[3] K. Sun, Y. Qian, and H.L. Jiang, "Metal-organic frameworks for photocatalytic water splitting and CO_2 reduction," *Angewandte Chemie International Edition*, Vol. 62, No. 15, Apr. 2023, https://doi.org/10.1002/anie.202217565

[4] S. Navarro-Jaén, M. Virginie, J. Bonin, M. Robert, R. Wojcieszak, and A. Y. Khodakov, "Highlights and challenges in the selective reduction of carbon dioxide to methanol," *Nature Reviews Chemistry*, Vol. 5, No. 8, pp. 564–579, Jun. 2021, https://doi.org/10.1038/s41570-021-00289-y

[5] S. Cheng et al., "Dual-defective two-dimensional/two-dimensional Z-scheme heterojunctions for CO_2 reduction," *ACS Catalysis*, Vol. 13, No. 11, pp. 7221–7229, Jun. 2023, https://doi.org/10.1021/acscatal.3c00219

[6] W. Zhang et al., "Progress of semiconductor nanomaterials in photocatalysis," *Development and Application of Materials*, Vol. 27, No. 3, pp. 92–96, 2012.

[7] X. Jiao et al., "Defect-mediated electron-hole separation in one-unit-cell ZnIn2S4 layers for boosted solar-driven CO2 reduction," *Journal of the American Chemical Society*, Vol. 139, No. 22, pp. 7586–7594, Jun. 2017, https://doi.org/10.1021/jacs.7b02290

[8] J. Wang, S. Lin, N. Tian, T. Ma, Y. Zhang, and H. Huang, "Nanostructured metal sulfides: classification, modification strategy, and solar-driven CO2 reduction application," *Advanced Functional Materials*, Vol. 31, No. 9, p. 2008008, Dec. 2020, https://doi.org/10.1002/adfm.202008008

[9] Y. He et al., "3D hierarchical $ZnIn_2S_4$ nanosheets with rich Zn vacancies boosting photocatalytic CO_2 reduction," *Advanced Functional Materials*, Vol. 29, No. 45, p. 19051, Sep. 2019, https://doi.org/10.1002/adfm.201905153

[10] C. Gao et al., "Heterogeneous single-atom catalyst for visible-light-driven high-turnover CO2 reduction: the role of electron transfer," *Advanced Materials*, Vol. 30, No. 13, p. e1704624, Feb. 2018, https://doi.org/10.1002/adma.201704624

[11] G. Wang, C.-T. He, R. Huang, J. Mao, D. Wang, and Y. Li, "Photoinduction of Cu single atoms decorated on UiO-66-NH_2 for enhanced photocatalytic reduction of CO_2 to liquid fuels," *Journal of the American Chemical Society*, Vol. 142, No. 45, pp. 19339–19345, Nov. 2020, https://doi.org/10.1021/jacs.0c09599

[12] J. Ding et al., "Single-atom silver-manganese catalysts for photocatalytic CO2 reduction with H2O to CH4," *Solar Energy Materials and Solar Cells*, Vol. 195, pp. 34–42, Jun. 2019, https://doi.org/10.1016/j.solmat.2019.02.009

[13] Y. Yang, F. Li, J. Chen, J. Fan, and Q. Xiang, "Single Au atoms anchored on amino-group-enriched graphitic carbon nitride for photocatalytic CO2 reduction," *ChemSusChem*, Vol. 13, No. 8, pp. 1979–1985, Apr. 2020, https://doi.org/10.1002/cssc.202000375

[14] J. Wan et al., "Defect effects on TiO2 nanosheets: stabilizing single atomic site Au and promoting catalytic properties," *Advanced Materials*, Vol. 30, No. 11, p. 17053, Jan. 2018, https://doi.org/10.1002/adma.201705369

[15] X. Li, J. Yu, M. Jaroniec, and X. Chen, "Cocatalysts for selective photoreduction of CO2 into solar fuels," *Chemical Reviews*, Vol. 119, No. 6, pp. 3962–4179, Mar. 2019, https://doi.org/10.1021/acs.chemrev.8b00400

[16] R. Pan et al., "Two-dimensional all-in-one sulfide monolayers driving photocatalytic overall water splitting," *Nano Letters*, Vol. 21, No. 14, pp. 6228–6236, Jul. 2021, https://doi.org/10.1021/acs.nanolett.1c02008

[17] X. Shi et al., "Protruding Pt single-sites on hexagonal ZnIn2S4 to accelerate photocatalytic hydrogen evolution," *Nature Communications*, Vol. 13, No. 1, pp. 1–10, Mar. 2022, https://doi.org/10.1038/s41467-022-28995-1

[18] Q. Li et al., "Fe isolated single atoms on S, N codoped carbon by copolymer pyrolysis strategy for highly efficient oxygen reduction reaction," *Advanced Materials*, Vol. 30, No. 25, pp. e1800588, May 2018, https://doi.org/10.1002/adma.201800588

[19] B. Qiao et al., "Single-atom catalysis of CO oxidation using Pt1/FeOx," *Nature Chemistry*, Vol. 3, No. 8, pp. 634–641, Jul. 2011, https://doi.org/10.1038/nchem.1095

[20] Y. Wang et al., "Single-atomic Cu with multiple oxygen vacancies on ceria for electrocatalytic CO_2 reduction to CH_4," *ACS Catalysis*, Vol. 8, No. 8, pp. 7113–7119, Aug. 2018, https://doi.org/10.1021/acscatal.8b01014